Biosensors and Bioelectronics 159 (2020) 112129

Contents lists available at ScienceDirect

Biosensors and Bioelectronics

journal homepage: http://www.elsevier.com/locate/bios

A transistor-based label-free immunosensor for rapid detection of tau protein

Miguel-Ángel García-Chamé, Óscar Gutiérrez-Sanz, Ebru Ercan-Herbst, Natalie Haustein, Marcin S. Filipiak, Dagmar E. Ehrnhöfer, Alexey Tarasov [*,1]

BioMed X Innovation Center, Im Neuenheimer Feld 515, 69120, Heidelberg, Germany

ARTICLE INFO

Keywords:
Alzheimer's disease
Tau protein
Field-effect transistors
Debye screening length
Immunosensor

ABSTRACT

Tau protein in cerebrospinal fluid (CSF) is a central and relevant biomarker of Alzheimer's disease (AD) that correlates with the severity of dementia. Unfortunately, so far, direct label-free detection of tau remains a challenge. Here, we present a transistor-based biosensor that detects the net charge of tau protein directly under physiological conditions. To achieve this, readily available whole anti-tau IgG antibodies are co-immobilized on the sensor surface with polyethylene glycol (PEG) molecules of different molecular weight. We show that by increasing the PEG size from 10 kDa to 20 kDa, the electrical response upon binding of tau improves significantly. These results support recent theoretical work that predicted larger PEGs to form a thicker surface layer with a higher detectable analyte charge. With 20 kDa PEG, we demonstrate label-free tau detection in a wide concentration range with detection limits <1 pM in 150 mM buffer and cell culture media, as well as < 10 pM in artificial CSF. This purely electrical method allows fast and simple tau detection within 30 min without sample processing, washing steps, or labeled detection antibodies. By exchanging the capture antibody, the platform is also amenable to different biomarkers and may enable future diagnostic tools for AD and other diseases.

1. Introduction

Alzheimer's disease (AD) is an age-related neurodegenerative disorder that gradually steals people's memories and abilities (Lord and Cruchaga, 2014; Sügis et al., 2019). Although some medications can minimize the symptoms of AD, so far, no treatment modifies the underlying course of the disease (Sügis et al., 2019). New therapeutic approaches for AD currently under development may be most effective at the beginning of the neurodegeneration process (Weller and Budson, 2018); however, the diagnostic criteria still depend on neurophysiological tests that consider progressive clinical symptoms that appear clearly after irreversible brain damage has already occurred (Jack et al., 2018). Therefore, despite recent advances in neuroimaging techniques to diagnose AD, there is an urgent need to improve the recognition of the disease for a successful therapeutic intervention (Hampel et al., 2018, 2010).

In the continuing need to identify patients with AD at an early stage for therapeutic trials, several biomarkers of AD have been identified. Among these biomarkers, amyloid-beta and tau proteins in cerebrospinal fluid (CSF) are widely accepted to diagnose AD (Blennow and Zetterberg, 2018). Tau is a protein that, in healthy conditions, binds to neuronal microtubules, promoting dynamism and stability (Qiang et al., 2018; Wang and Mandelkow, 2016). In the brains of people with AD, tau undergoes complex post-translational modifications (PTMs) that cause its dissociation from microtubules and aggregation into paired helical filaments, which finally form neurofibrillary tangles (NFTs) in the neuronal soma (Wang and Mandelkow, 2016). As NFTs accumulate, their abundance in the brain increases, compromising the normal function of neurons and eventually leading to cell death (Congdon and Sigurdsson, 2018). Because tau is actively secreted by neurons, both in its unmodified state and with PTMs, specific measurements of tau PTMs, such as tau phosphorylation, can serve as additional significant biomarkers (Blennow and Zetterberg, 2018). In this line, the total level of tau in CSF correlates with neurodegeneration in AD, making it a good predictor of AD symptoms (Masters et al., 2015).

Tau detection is generally carried out with immunoassays such as enzyme-linked immunosorbent assay (ELISA) (Kang et al., 2013; Scarano et al., 2016). More recently, new strategies have been proposed that

* Corresponding author.
E-mail addresses: tarasov@bio.mx, alexey.tarasov@hs-kl.de (A. Tarasov).
[1] Present address: Kaiserslautern University of Applied Sciences, Amerikastr. 1, 66482 Zweibrücken, Germany.

https://doi.org/10.1016/j.bios.2020.112129
Received 15 November 2019; Received in revised form 5 February 2020; Accepted 28 February 2020
Available online 4 March 2020

include electrochemistry and surface plasmon resonance (SPR) (Scarano et al., 2016; Shui et al., 2018). While these methods are now used in clinical trials, they suffer from inherent disadvantages such as being time-consuming, laborious, or insufficiently sensitive (Xia et al., 2016). For example, ELISA is a multi-step process that involves mixing, blocking, incubation, and several washing steps (Qin et al., 2018). Regardless of future improvements, immunoassays designed to quantify tau should guarantee a sufficiently high sensitivity because significant cut-off values of tau for AD are quite low, and vary between 200 and 400 pg/ml (≈3.6–7.3 pM) in the CSF (Palmqvist et al., 2019).

Field-effect transistors (FET) are transducers that offer a possible alternative solution for biomarker detection with high sensitivity, in addition to providing ease of operation, real-time detection, and low cost (Kaisti, 2017). In general, FET-based biosensors measure changes in surface potential as charged molecules interact with the sensor surface. This technology can reliably detect small and densely charged species, such as protons, metal ions, and DNA. However, the widespread use for the detection of larger and less densely charged molecules, namely proteins, is limited due to the high number of electrolyte ions in physiological samples. Briefly, mobile ions in biological solutions can screen the analyte charge while it binds to the sensor surface (known as the Debye screening effect). Consequently, the effective distance where the transducer can detect a specific molecule by its intrinsic charge is of crucial importance and is defined by the Debye length. This distance is less than 1 nm from the surface in solutions with high ionic strength (~150 mM ionic strength), so that the further away the target species is from the detection surface, the lower the sensor response (Haustein et al., 2019; Kaisti, 2017).

FET-based biosensors with short capture molecules, such as antibody fragments, nanobodies or aptamers, co-immobilized with poly(ethylene glycol) (PEG) on their surface have recently overcome this problem, increasing the effective signal while detecting proteins even in high ionic strength environments (Andoy et al., 2018; Filipiak et al., 2018; Gao et al., 2016; Gutiérrez-Sanz et al., 2017). More recently, it was proposed that the co-immobilized PEG improves the sensor response by creating a surface layer with a virtually constant potential (Donnan potential). Within this layer, the potential is nearly independent of the ionic strength, resulting in a higher detectable analyte charge (Haustein et al., 2019). In theory, this surface layer could be extended using longer PEG molecules to further improve the FET response, especially if relatively large capture molecules (such as whole IgG antibodies) or protein analytes are of interest. So far, however, most experimental research has focused on one particular PEG size (10 kDa) that may not be suitable for all antigen-receptor pairs.

Here, we first show that the 10 kDa PEG is not sufficient to overcome the Debye length limitation if whole IgG antibodies are used, most likely due to their large size. We then demonstrate that by increasing the PEG size to 20 kDa, substantial signals can be obtained upon analyte binding even in undiluted physiological solutions. These results are in line with recent theoretical predictions and provide important insights into the effect of PEG size on the sensor response. As a proof-of-concept, we explore this method for the label-free detection of a relevant biomarker of AD, tau protein, in different physiological solutions. By combining a specific surface chemistry with our previously published differential readout scheme (Gutiérrez-Sanz et al., 2019), it is shown that tau detection limits are < 1 pM in 150 mM buffer and neuronal cell culture media, and <10 pM in artificial CSF (aCSF). To the best of our knowledge, this is the first report on the highly sensitive and label-free detection of tau protein directly in undiluted complex samples while using a whole IgG antibody in a FET-based biosensor.

2. Materials and methods

Chemicals: Ammonia solution (NH_3 (aq)) 25%, calcium chloride ($CaCl_2$), di-sodium hydrogen phosphate (Na_2HPO_4), ethanol (99%), 30% hydrogen peroxide (H_2O_2), magnesium chloride ($MgCl_2$), potassium chloride (KCl), sodium chloride (NaCl), sodium dihydrogen phosphate (NaH_2PO_4), were purchased from Carl Roth GmbH + Co. KG (Germany). 2-(N-Morpholino)ethanesulfonic acid (MES) hydrate, 1-ethyl-3-(3-(dimethylamino)-propyl) carbodiimide hydrochloride (EDC-HCl), and *N*-hydroxysuccinimide (NHS) were purchased from Sigma-Aldrich Co. LLC (Germany). Thiolated poly(ethylene glycol) (mPEG-thiol, PEG) (10 kDa and 20 kDa) was purchased from Creative PEG-Works (USA), and bifunctional thiolated and carboxylated poly (ethylene glycol) (COOH-EG_8-thiol, linker) was purchased from Celares GmbH (Germany). Thiolated molecules were stored at −20 °C under inert conditions and prepared fresh for each experiment to ensure the reduced form of the thiols.

Biomolecules: Anti-tau IgG mouse monoclonal HT7 antibody (stored in PBS) was purchased from Thermo Fischer Scientific (Germany). The IgG antibody detects all isoforms of tau by an epitope composed of amino acids 159 to 163 (of 441 amino acids in a full-length tau). With a positive net charge at pH 7.4 (isoelectric point 8.6), full-length tau protein was recombinantly expressed in *E. coli* strain as previously described (Ercan et al., 2017) and stored in 50 mM sodium phosphate buffer pH 7.0, 1 mM ethylene glycol bis(β-aminoethyl)-ether) *N,N,N',N'* tetraacetic acid (EGTA), and 1 mM 1,4-dithiothreitol (DTT). Bovine serum albumin (BSA) was purchased from Carl Roth GmbH + Co. KG (Germany).

Artificial cerebrospinal fluid (aCSF): aCSF was prepared in-house following a published protocol (Liu et al., 2013) and comprised 150 mM NaCl, 3.0 mM KCl, 1.4 mM $CaCl_2$, 0.8 mM $MgCl_2$, 1.0 mM sodium phosphate (0.8 mM Na_2HPO_4 and 0.2 mM NaH_2PO_4), and 3 μM BSA. The pH was adjusted to 7.4 with NaOH.

Neuronal cell culture media: It consisted of N2B27 Media (50% DMEM/F-12 and 50% Neurobasal solution: 1:200 N2, 1:100 B27, 1% PenStrep, and 0.5 mM nonessential amino acids) (all from Invitrogen, Germany), with a pH of 7.4.

Sensor fabrication: Glass slides (25 × 25 mm; Borofloat 33, Schott) were coated with Ti (10 nm thick) and Au (100 nm thick) by thermal evaporation through a shadow mask to create electrodes of 0.55 mm × 0.75 mm exposed to the liquid sample. The evaporation was carried out at InnovationLab GmbH, Heidelberg.

Sensor modification: Gold sensors comprising active and control electrodes were immersed in a "basic" Piranha solution (5:1:1 vol mixture of deionized water, 30% H_2O_2, and 25% NH_3) for 15 min at 80 °C. Then gold was rinsed with deionized water, dried with N_2, and treated with UV/ozone and O_2 plasma for 10 min, respectively. All modification steps were carried out at 21 ± 2 °C and at a flow rate of 80 μl/min, unless otherwise stated. After mounting a microfluidic chamber onto the gold sensor, the sensor electrodes were rinsed with buffer (50 mM MES pH 7.0) for 10 min and then incubated in a mixed solution of 1 μM of thiolated PEG (10 kDa or 20 kDa) and 40 μM of linker (0.5 kDa COOH-EG_8-thiol) for 60 min (1:40 M ratio PEG:linker). Subsequently, the sensor was rinsed with buffer for 10 min to remove excess unbound PEG. The carboxyl group of the linker was activated by incubating the sensors in a solution of 0.4 mg/ml EDC and 0.6 mg/ml NHS in 50 mM MES (pH 4.5) for 20 min. Once activated, active electrodes were incubated with anti-tau antibody (8 μg/ml) and controls with a solution of BSA (1.4 mg/ml), both in 50 mM MES (pH 4.5), for 80 min without flow. Excess antibodies and BSA were removed by rinsing with buffer for 10 min. To prevent non-specific adsorption, the remaining surface binding sites (not covered by antibodies or BSA) were blocked by incubating the sensors in a 10 mg/ml BSA solution for 10 min. Lastly, electrodes were rinsed with buffer for 20 min.

Extended-gate FET measurements: Fig. S3A shows the sensor readout schematically with an extended-gate connection separating the sensing electrodes and gate terminals of commercial MOSFETs (Microchip Technology). An Ag/AgCl reference electrode (Dri-REF, World Precision Instruments) was placed near the sensor surface to apply constant gate potentials. Electrical measurements were carried out with a dual-channel source meter (Keithley 2636 B). Characteristic transfer curves

of each modified electrode were obtained by monitoring the drain-source current (I_{ds}) at constant potential (V_{ds} = 0.1 V) while sweeping the potential applied at the reference electrode (V_{ref}) from -0.0 to -0.9 V (typical transfer curves are shown in Fig. S3B). For real-time measurements, a potential of -0.3 V was applied to the reference electrode and I_{ds} was monitored over time at a fixed V_{ds} = 0.1 V. The measured current (sensor output I_{ds}) was recalculated to potential changes (ΔV) by using the transconductance (slope of the transfer curve: slope = I_{ds}/V_{ref}), recorded prior to real-time measurements. Samples were passed through the sensor electrodes using a syringe pump (Aladdin AL4000-220Z, World Precision Instruments, Germany), with tau binding monitored for 30 min at 37 °C.

Differential readout: A differential measurement was obtained by subtracting the signal of the control (BSA modified) from the respective active (IgG modified) electrode (see Fig. S3C). By doing that, we can correct effects such as time-dependent drift, changes in pH or ionic strength, and electrical fluctuation of the measurement set-up as described in our previous work (Gutiérrez-Sanz et al., 2019). Additionally, to get a stable baseline, we measured "blank" samples before introducing samples containing tau. The sensor response towards tau was obtained using the potential shifts (ΔV) measured after 25 min in contact with the sample spiked with tau (Fig. S4 shows an example of this measurement).

QCM measurements: Quartz crystal microbalance (QCM) measurements were carried out with a QSense Analyzer on gold-coated QCM crystals (fundamental frequency of 4.95 MHz) from Biolin Scientific AB, Sweden. The QCM crystals were cleaned in "basic" Piranha solution for 15 min at 80 °C, rinsed with deionized water, dried with N_2, and treated with UV/ozone for 10 min. The surface modification and tau sensing were carried out under flow conditions (80 μl/min) using a peristaltic pump (IPC 4, ISMATEC GmbH, Germany).

3. Results and discussion

The co-immobilization of PEG together with short capture molecules targeting protein analytes has recently overcome the Debye screening limitation and improved the sensor response without the need for washing or desalting steps. In particular, the use of 10 kDa PEG on a detection surface has already increased electrical signals compared to a control surface without PEG upon immunodetection of thyroid stimulating hormone (TSH) with anti-TSH F(ab')$_2$ antibody fragments (Gutiérrez-Sanz et al., 2017). Haustein et al. proposed that the PEG introduced during the sensor modification steps increased the sensor signals by creating a surface layer with an almost constant potential, surrounding the capture molecules (e.g., a F(ab')$_2$ fragment) and the target analyte (e.g., a charged protein) (Haustein et al., 2019). Therefore, analyte charges interacting with immobilized capture molecules within the surface layer are likely to produce a detectable signal that is enhanced in the presence of PEG. The effect of PEG on the detectable analyte charge was described with an analytical model that can estimate the sensor response based on the available capture molecule and the analyte of interest (Haustein et al., 2019). This model proposed that, to yield a high sensor response, the PEG used on the sensor surface should be at least as long as the combined lengths of the capture molecules and the linker molecules that tether them on the surface, plus the size of the analyte of interest. Then, despite the strong screening effect associated with the presence of large capture molecules (Kaisti, 2017), a FET-based biosensor with IgG antibodies could be conveniently designed by adapting the surface layer with a PEG whose size improves the sensor signals. To experimentally prove this hypothesis and develop a useful tool for AD research and diagnosis, we chose a readily available anti-tau IgG antibody to design a biosensor that can detect tau protein under physiological conditions.

3.1. Surface layer design

In the surface layer design, we considered the length of an antibody to be 12 nm (Pollitt et al., 2015; Yeow et al., 2017). The length of the linker molecules (0.5 kDa COOH-EG$_8$-SH) used here was approximately 2.4 nm (Haustein et al., 2019). When an antibody and a linker molecule form a complex that is perpendicularly straight from the surface, the maximum estimated height would be around 14.4 nm. To form a surface layer that allows a high sensor response, PEG must cover such distance. Therefore, we chose a long 20 kDa PEG because the approximate length of this molecule was measured to be 18 nm (Emilsson et al., 2015). Although this previous measurement was performed in PBS (phosphate-buffered saline), it is expected to be comparable to the height of PEG obtained in MES buffer and, based on our liquid AFM data, the immobilized PEG is in a brush-like regime (Haustein et al., 2019). Therefore, 20 kDa PEG will be larger than the combined lengths of the linker, the antibody, and tau. As a result, we expect to measure most of the tau charge because tau most likely binds to the anti-tau antibody within the surface layer. For comparison, based on the PEG-induced signal enhancement produced by 10 kDa PEG in previous works (Andoy et al., 2018; Filipiak et al., 2018; Gao et al., 2016; Gutiérrez-Sanz et al., 2017), we also prepared sensors with this shorter PEG. The 10 kDa PEG has a theoretical length of 11 nm (Emilsson et al., 2015; Haustein et al., 2019). Since this is at least 3 nm shorter than the linker-antibody complex, we expect that most tau binding sites will be outside the three-dimensional surface layer. Consequently, electrolyte ions would likely screen the charges carried by amino acids of tau because the surface layer produced by short PEG molecules would not significantly reduce this effect.

To experimentally investigate the designed surface layers, we used a sensor layout comprising a chip with two electrodes, called "active" (IgG modified) and "control" (BSA modified), as shown in Fig. 1A. We prepared several sensors with different surface layers by first co-immobilizing linker molecules with 10 kDa PEG or 20 kDa PEG on both electrodes, then introducing anti-tau IgG antibodies on the active

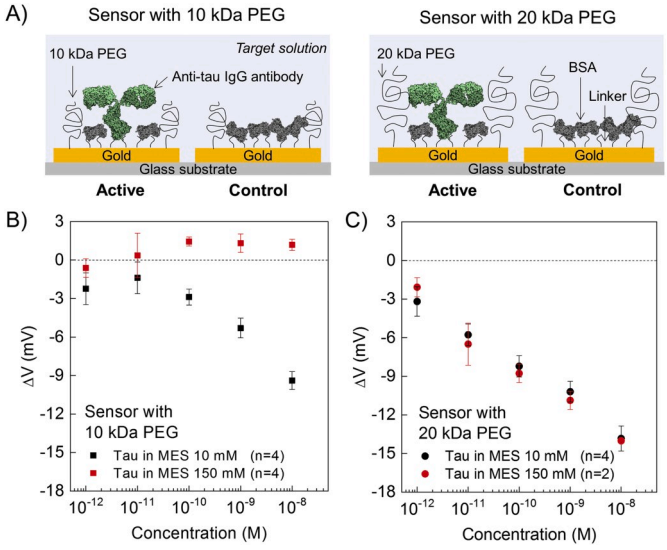

Fig. 1. Schematic representation of the sensor, and the measured response to tau. A) The extended-gate gold electrodes with different surface modifications comprising either 10 kDa PEG (left panel) or 20 kDa PEG (right panel). Each sensing system had an active electrode that contained anti-tau antibodies and a control passivated with non-interacting BSA. The overall readout signal was the difference between these electrodes (active – control). Calibration curves of sensors with B) 10 kDa PEG and C) 20 kDa PEG. Sensor responses were measured in low and high ionic strength buffers using 10 mM and 150 mM MES (pH 7.4), respectively. The dashed line represents the baseline of the differential signal obtained in blank samples. (For interpretation of the references to colour in this figure legend, the reader is referred to the Web version of this article.)

side and BSA on the control. Immobilization of the specific antibody or the blocking agent BSA was the only modification step in which the electrodes differed. The surface modification protocol was optimized using quartz crystal microbalance (QCM) with details provided in the supplementary material (Fig. S1). During QCM studies, we found that tau binding improved with increasing temperature. Therefore, all electrical measurements in this work were performed at 37 °C instead of 22 °C (Fig. S2). After the functionalization, we connected each electrode to the gate terminal of a MOSFET and measured them at the same time ("extended-gate configuration") (Gutiérrez-Sanz et al., 2017, 2019; Tarasov et al., 2015, 2016). Details of the electrical connection can be found in Fig. S3A. Because the active and control substrates always shared the same solutions, we calculated the specific tau-related signal of each sensor through a differential measurement between the active and control electrodes that accounts for the non-specific events (Gutiérrez-Sanz et al., 2019) (Fig. S3 and Fig. S4). Also, blank controls were introduced before samples containing tau to calibrate and characterize the sensor response.

3.2. Sensor response

First, as shown in Fig. 1B, a calibration curve was recorded using sensors with 10 kDa PEG at low ionic strength buffer (10 mM MES) to reduce the ion screening effect. As we subtracted the control from its corresponding active electrode, the potential shifts ranged from -2 mV to -10 mV starting from the lowest (1 pM) to the highest (10 nM) tau concentration tested, respectively. The sensor responded with more sensitivity to tau concentrations greater than 100 pM. However, by repeating the experiments in a high ionic strength buffer (150 mM MES), we could not detect tau reliably because measured signals lacked a clear trend as tau concentrations increased. These results confirm that sensors with 10 kDa PEG are not suitable for tau detection at high ionic strength when a whole IgG antibody is the capture molecule on the surface.

Since we hypothesized that a thicker surface layer achieved by applying longer PEG molecules may increase the sensor response, we prepared electrodes with a more pronounced surface layer using 20 kDa PEG, as shown in Fig. 1C. By increasing the PEG size to 20 kDa, the sensor signal in 10 mM MES buffer increased on average by 2 mV for each tenfold tau concentration increase and reached a value of -14 mV for 10 nM tau. Tau was reliably detected even in high ionic strength buffer (150 mM MES). Here, the lowest and highest tau concentration had a signal of -2 mV to -14 mV, respectively. Notably, we did not find a significant difference between the tau signals measured in 10 mM and 150 mM buffer, suggesting that the presence of 20 kDa PEG on the surface increased the surface layer to a level that effectively reduced the Debye screening. Assuming constant dimensions of tau protein and its capture IgG antibody within both surface layers containing either 10 kDa or 20 kDa PEG, we conclude that the improved detectable signal, observed in sensors with 20 kDa PEG, was mainly due to the thicker surface layer generated by this longer PEG.

After validating the sensor response in 150 mM MES buffer and showing that 20 kDa PEG improves the detectable signal, we evaluated the sensor performance in complex matrixes for future applications. These experiments included measuring tau from cell culture media to facilitate tau detection in a research setting and quantification of tau in aCSF as an important step towards diagnosis with human samples. Therefore, we first spiked tau into fresh neuronal cell culture media to mimic the secretion of tau from cultured neurons (Pooler et al., 2013). Fig. 2A shows the sensor response under these conditions. The sensor signals here changed approximately by 3 mV per order of magnitude as the tau concentration increased, reaching -15.0 ± 0.2 mV for 10 nM tau. Despite the higher device-to-device variation, it was possible to detect tau as its concentration increased in this solution made of various salts, amino acids, vitamins, and antibiotics. We calculated the lower limit of detection (LoD) as LoD = $\Delta V_B \pm 3 \times SD_B$, where ΔV_B is the mean signal obtained in 12 blank samples without tau. Fig. 2A represents these data

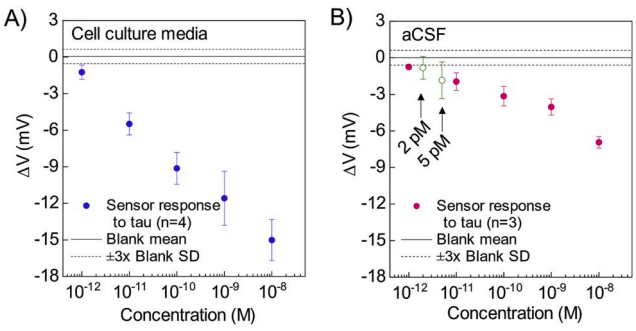

Fig. 2. Calibration curves of sensors with 20 kDa PEG in complex solutions: A) fresh cell culture media and B) aCSF. The horizontal lines represent the baseline fluctuations (mean value and 3×SD_B of the differential signal measured with sensors exposed to blank samples). Arrows in B) and open symbols show additional measurements around 3 pM, which is a relevant cut-off value of tau in CSF.

through horizontal lines: $\Delta V_B = 5.3 \times 10^{-5}$ V, $SD_B = 2.0 \times 10^{-4}$ V, and 3 × SD_B = 0.6 mV. Because 1 pM tau yielded a signal of -1.2 ± 0.6 mV, we conclude that tau concentrations above 1 pM can be reliably distinguished from the baseline in neuronal cell culture media.

We next measured tau in aCSF, which adequately mimics the physiological properties of the CSF (Spector et al., 2015), again using sensors with 20 kDa PEG (Fig. 2B). Testing the sensor performance in this sample type is relevant because the total levels of tau in CSF reflect the intensity of neuronal damage, correlating with the severity of the neurogenerative process in AD (Blennow et al., 2010). Qualitatively, measurements in aCSF showed a clear response upon the addition of tau, but the electrical signal reached only half of the values measured with 150 mM buffer and cell culture media. For example, the response to 10 nM tau in aCSF (-7.0 ± 0.5 mV) was half of the signal obtained in 150 mM buffer (-14.0 ± 0.2 mV). Unlike the previously used solutions, aCSF contains a very high concentration of protein BSA. Therefore, we believe that the detectable signal decreased mostly because of a partial blocking of the surface by BSA present in aCSF, an effect that could be critical for predicting the sensor response in human CSF, which contains a mix of different proteins (Spector et al., 2015).

In a follow-up experiment, the sensor response was measured with samples spiked with 2 pM and 5 pM tau to test if the sensor could discriminate a clinically relevant mean value of tau in healthy subjects, such as 3 pM (Scarano et al., 2016). Our results did not show a significant difference between the signals of these two concentrations as indicated by the error bars (see arrows in Fig. 2B). Consequently, 21 different sensors were measured after being exposed to aCSF to estimate the ΔV_B and calculate the LoD. Horizontal lines represent these data in Fig. 2B: $\Delta V_B = -8.5 \times 10^{-20}$ V, $SD_B = 2.0 \times 10^{-4}$ V, and 3 × SD_B = 0.6 mV. Accordingly, only tau concentrations above 10 pM can be reliably distinguished from the baseline after 25 min of sample incubation, indicating a LoD of ≈10 pM in aCSF. For comparison, the detection limit was around 1 pM in cell culture media and clearly below 1 pM in 150 mM buffer, which covered significant reference values of tau that can be as low as 3.6 pM for mild cognitive impairment and 7.3 pM for dementia (Palmqvist et al., 2019).

3.3. Future work and comparison with the state of the art

Additional research is required to further improve the precision and the detection limit in aCSF. Here, we have neglected the random orientation of the antibody, which could be in a position that prevents the analyte from binding to the epitope or being inside the surface layer. Site-specific antibody immobilization may, therefore, offer an opportunity for future improvement. In practice, tau measurements with immunoassays pose a challenge because tau in the human CSF is commonly

Table 1
Selected techniques for tau detection.

Transducer	Specific technique[(A)]	Medium used to read out tau signal	Sandwich immunoassay	LoD[(B)]	Label	Signal amplification	Available on market	Approximate total assay time	Ref.
Optical	Electrochemiluminescence	Buffer	YES	1.07 - 23.7 pg/ml ≈430 fM	YES	NO	YES	>2 h	Meso Scale Diagnostics, n.d.
	Spectro-photometry/ inter-ferometry	Buffer, CSF[(C)]	NO	15.6 pg/ml ≈284 fM (in buffer)	NO	NO	NO	<20 min	Song et al., (2018)
	LSPR	Buffer	NO	10 pg/ml ≈180 fM	NO	NO	NO	1 h	Vestergaard et al., (2008)
	LSPR	Ultrapure water	NO	100 fM	NO	YES	NO	1 h	Kim et al., (2019)
	LSPR	Ultrapure Water	NO	23.6 fM	NO	NO	NO	1 h	Kim et al., (2018)
Electrochemical	DPV and EIS	Diluted serum, CSF	YES	0.15 nM	NO	YES[(D)]	NO	<30 min	Derkus et al., (2017)
	DPV	Serum	NO	0.968 pM	NO	YES[(D)]	NO	30 min	Dai et al., (2019)
	CV and EIS	Buffer, serum	NO	0.03 pM	NO	YES[(D)]	NO	<1 h	Wang et al., (2017)
Potentiometric	FET	Buffer, CCM[(E)], aCSF	NO	<1 pM, 1 pM, 10 pM	NO	NO	NO	<30 min	**THIS WORK**

(A) Abbreviations: LSRP = localized surface plasmon resonance; DPV = differential pulse voltammetry; EIS = electrochemical impedance spectroscopy; CV = cyclic voltammetry; FET = field effect transistor. (B) Approximate molar concentration of tau calculated using a molecular weight of 55 kDa. (C) The group only reported the viability of the sensor to detect tau in CSF with a multiplexed readout. (D) The readout signal derived in the presence of electroactive species such as $[Fe(CN)_6]^{3-/4-}$. (E) CCM = neuronal cell culture media.

fragmented (Blennow and Zetterberg, 2018), which may even cause a loss of the epitope that recognizes the chosen antibody. In our case, tau fragments would influence the electrical signal due to their unforeseen size that changes the number of charged amino acids detected in the surface layer. Likewise, tau presents PTMs that can potentially modify its native net charge (Alonso et al., 2018). All these factors may result in an underestimation of the actual concentration. Regardless of future optimization work, the improvement of the sensor response by using 20 kDa PEG remains significant, and the detection limit obtained in cell culture media is remarkable.

To the best of our knowledge, this is the first attempt to detect tau with a purely electrical device by using the effect of PEG size to extend the Debye length above its expected limits. This strategy allowed the integration of a readily available capture IgG antibody into a FET-based biosensor to finally allow direct protein detection in unprocessed samples. With theoretical knowledge about the effect of PEG on the ionic screening of analyte charges, we avoid the need for short capture molecules such as aptamers (Gao et al., 2016), nanobodies (Filipiak et al., 2018), and antibody fragments (Andoy et al., 2018; Gutiérrez-Sanz et al., 2019). Importantly, we extend the application space of FET biosensors to whole size antibodies that currently still are the standard capture molecules in diagnostics and research. Other works that detected tau have used electrochemical, optical, or mass-sensitive techniques and most of them in a sandwich immunoassay approach. Table 1 summarizes some relevant publications, including a commercial kit for the detection of tau (Meso Scale Discovery). Table S2 (in the SI) presents, in more detail, these and other works that have also quantified tau. Unlike these technologies, our approach is the only one capable of fast (<30 min) detection of tau without sample dilution, washing steps, or labeled detection antibodies. The optical sensor with the most similar performance to the present work still depends on complex instrumentation and translucent components coupled to specific lenses to allow quantification of tau in CSF (Song et al., 2018). Therefore, our technology benefits from fewer reagents, shorter detection times, and lower overall costs. In this line, the presented biosensor offers versatility, and may also enable the detection of various other AD biomarkers. For example, the capture antibody used here could be replaced by a different antibody against a specific post-translationally modified tau. We believe that this technology can become a viable platform for the detection of AD biomarkers and can be useful for clinical diagnosis and research purposes.

4. Conclusions

An extended-gate FET-based biosensor was developed for tau detection under physiologically relevant conditions without the need for sample processing. This was achieved by tailoring the sensor surface with a suitable PEG size covering the entire combined lengths of the whole IgG antibody, chosen as the capture molecule, and tau as the target analyte. We showed that sensors containing 20 kDa PEG are more sensitive than sensors constructed with 10 kDa PEG for direct tau detection, overcoming the theoretical Debye screening limitation, even when whole antibodies are used. We validated the sensor performance by measuring tau in samples that mimic frequent applications, such as neuronal cell culture media for scientific research and aCSF for medical diagnostics, obtaining an approximate LoD of 1 pM and 10 pM, respectively. Thus, the transistor-based biosensor offers a new alternative for measuring tau in real time without optical readout and sample pre-treatment. Ultimately, it may yield a versatile platform for the detection of many other biomarkers in clinical practice.

Declaration of competing interest

The authors declare that they have no known competing financial interests or personal relationships that could have appeared to influence the work reported in this paper.

CRediT authorship contribution statement

Miguel-Ángel García-Chamé: Conceptualization, Methodology, Investigation, Formal analysis, Writing - original draft. **Óscar Gutiérrez-Sanz:** Conceptualization, Software, Supervision, Writing - review & editing. **Ebru Ercan-Herbst:** Conceptualization, Supervision, Writing - review & editing. **Natalie Haustein:** Software, Writing - review & editing. **Marcin S. Filipiak:** Resources, Writing - review & editing. **Dagmar E. Ehrnhöfer:** Conceptualization, Supervision, Writing - review & editing. **Alexey Tarasov:** Conceptualization, Supervision, Writing - review & editing.

Acknowledgments

The authors thank Dr. Kim Remans and Dr. Jacob Scheurich at the EMBL protein purification core facility for the expression and purification of recombinant tau protein, and Amy Leson for her assistance during the sensor platform design.

Appendix A. Supplementary data

Supplementary data to this article can be found online at https://doi.org/10.1016/j.bios.2020.112129.

Funding

The research teams “Nanomaterial-Based Biosensors” (MGC, OGS, NH, MSF, AT) and “Tau-mediated Neurodegeneration in Alzheimer’s disease” (EEH, DEE), both at BioMed X Innovation Center, were kindly sponsored by Roche Diagnostics GmbH and AbbVie GmbH & Co KG, respectively. The sponsors played no role in study design, data collection and analysis, preparation of the manuscript, or decision to publish.

References

Alonso, A.D., Cohen, L.S., Corbo, C., Morozova, V., ElIdrissi, A., Phillips, G., Kleiman, F. E., 2018. Front. Cell. Neurosci. 12, 338.
Andoy, N.M., Filipiak, M.S., Vetter, D., Gutiérrez-Sanz, Ó., Tarasov, A., 2018. Adv. Mater. Technol. 3, 1800186.
Blennow, K., Hampel, H., Weiner, M., Zetterberg, H., 2010. Nat. Rev. Neurol. 6, 131–144.
Blennow, K., Zetterberg, H., 2018. J. Intern. Med. 284, 643–663.
Congdon, E.E., Sigurdsson, E.M., 2018. Nat. Rev. Neurol. 14, 399–415.
Dai, Y., Chiu, L.Y., Chen, Y., Qin, S., Wu, X., Liu, C.C., 2019. ACS Sens. 4, 161–169.
Derkus, B., Acar Bozkurt, P., Tulu, M., Emregul, K.C., Yucesan, C., Emregul, E., 2017. Biosens. Bioelectron. 89, 781–788.
Emilsson, G., Schoch, R.L., Feuz, L., Höök, F., Lim, R.Y.H., Dahlin, A.B., 2015. ACS Appl. Mater. Interfaces 7, 7505–7515.
Ercan, E., Eid, S., Weber, C., Kowalski, A., Bichmann, M., Behrendt, A., Matthes, F., Krauss, S., Reinhardt, P., Fulle, S., Ehrnhoefer, D.E., 2017. Mol. Neurodegener. 12, 87.
Filipiak, M.S., Rother, M., Andoy, N.M., Knudsen, A.C., Grimm, S., Bachran, C., Swee, L. K., Zaumseil, J., Tarasov, A., 2018. Sensor. Actuator. B Chem. 255, 1507–1516.
Gao, N., Gao, T., Yang, X., Dai, X., Zhou, W., Zhang, A., Lieber, C.M., 2016. Proc. Natl. Acad. Sci. U.S.A. 113, 14633–14638.
Gutiérrez-Sanz, Ó., Andoy, N.M., Filipiak, M.S., Haustein, N., Tarasov, A., 2017. ACS Sens. 2, 1278–1286.
Gutiérrez-Sanz, Ó., Haustein, N., Schroeter, M., Oelschlaegel, T., Filipiak, M.S., Tarasov, A., 2019. Sensor. Actuator. B Chem. 295, 153–158.
Hampel, H., Frank, R., Broich, K., Teipel, S.J., Katz, R.G., Hardy, J., Herholz, K., Bokde, A.L.W., Jessen, F., Hoessler, Y.C., Sanhai, W.R., Zetterberg, H., Woodcock, J., Blennow, K., 2010. Nat. Rev. Drug Discov. 9, 560–574.
Hampel, H., O’Bryant, S.E., Molinuevo, J.L., Zetterberg, H., Masters, C.L., Lista, S., Kiddle, S.J., Batrla, R., Blennow, K., 2018. Nat. Rev. Neurol. 14, 639–652.
Haustein, N., Gutiérrez-Sanz, Ó., Tarasov, A., 2019. ACS Sens. 4, 874–882.
Jack, C.R., Bennett, D.A., Blennow, K., Carrillo, M.C., Dunn, B., Haeberlein, S.B., Holtzman, D.M., Jagust, W., Jessen, F., Karlawish, J., Liu, E., Molinuevo, J.L., Montine, T., Phelps, C., Rankin, K.P., Rowe, C.C., Scheltens, P., Siemers, E., Snyder, H.M., Sperling, R., Elliott, C., Masliah, E., Ryan, L., Silverberg, N., 2018. Alzheimer’s Dementia 14, 535–562.
Kaisti, M., 2017. Biosens. Bioelectron. 98, 437–448.
Kang, J.H., Korecka, M., Toledo, J.B., Trojanowski, J.Q., Shaw, L.M., 2013. Clin. Chem. 59, 903–916.
Kim, H., Lee, J.U., Kim, S., Song, S., Sim, S.J., 2019. ACS Sens. 4, 595–602.
Kim, H., Lee, J.U., Song, S., Kim, S., Sim, S.J., 2018. Biosens. Bioelectron. 101, 96–102.
Liu, L., Zhao, F., Ma, F., Zhang, L., Yang, S., Xia, N., 2013. Biosens. Bioelectron. 49, 231–235.
Lord, J., Cruchaga, C., 2014. Nat. Neurosci. 17, 1138–1140.
Masters, C.L., Bateman, R., Blennow, K., Rowe, C.C., Sperling, R.A., Cummings, J.L., 2015. Nat. Rev. Dis. Prim. 1, 15056.
Scale Diagnostics. URL. https://www.mesoscale.com/~/media/files/product%20inserts/human%20total%20tau.pdf. accessed 03.12.2019.
Palmqvist, S., Janelidze, S., Stomrud, E., Zetterberg, H., Karl, J., Zink, K., Bittner, T., Mattsson, N., Eichenlaub, U., Blennow, K., Hansson, O., 2019. JAMA Neurol 76, 1060–1069.
Pollitt, M.J., Buckton, G., Piper, R., Brocchini, S., 2015. RSC Adv. 5, 24521–24527.
Pooler, A.M., Phillips, E.C., Lau, D.H.W., Noble, W., Hanger, D.P., 2013. EMBO Rep. 14, 389–394.
Qiang, L., Sun, X., Austin, T.O., Muralidharan, H., Jean, D.C., Liu, M., Yu, W., Baas, P.W., 2018. Curr. Biol. 28, 2181–2189.e4.
Qin, J., Jo, D.G., Cho, M., Lee, Y., 2018. Biosens. Bioelectron. 113, 82–87.
Scarano, S., Lisi, S., Ravelet, C., Peyrin, E., Minunni, M., 2016. Anal. Chim. Acta 940, 21–37.
Shui, B., Tao, D., Florea, A., Cheng, J., Zhao, Q., Gu, Y., Li, W., Jaffrezic-Renault, N., Mei, Y., Guo, Z., 2018. Biochimie 147, 13–24.
Song, C., Deng, P., Que, L., 2018. Nanomed. Nanotechnol. Biol. Med. 14, 1845–1852.
Spector, R., Robert Snodgrass, S., Johanson, C.E., 2015. Exp. Neurol. 273, 57–68.
Sügis, E., Dauvillier, J., Leontjeva, A., Adler, P., Hindie, V., Moncion, T., Collura, V., Daudin, R., Loe-Mie, Y., Herault, Y., Lambert, J.-C., Hermjakob, H., Pupko, T., Rain, J.-C., Xenarios, I., Vilo, J., Simonneau, M., Peterson, H., 2019. Sci. Data 6, 151.
Tarasov, A., Gray, D.W., Tsai, M.Y., Shields, N., Montrose, A., Creedon, N., Lovera, P., O’Riordan, A., Mooney, M.H., Vogel, E.M., 2016. Biosens. Bioelectron. 79, 669–678.
Tarasov, A., Tsai, M.Y., Flynn, E.M., Joiner, C.A., Taylor, R.C., Vogel, E.M., 2015. 2D Mater. 2, 44008.
Vestergaard, M., Kerman, K., Kim, D.K., Hiep, H.M., Tamiya, E., 2008. Talanta 74, 1038–1042.
Wang, S.X., Acha, D., Shah, A.J., Hills, F., Roitt, I., Demosthenous, A., Bayford, R.H., 2017. Biosens. Bioelectron. 92, 482–488.
Wang, Y., Mandelkow, E., 2016. Nat. Rev. Neurosci. 17, 5–21.
Weller, J., Budson, A., 2018. F1000Research 7, p. F1000. Faculty Rev-1161.
Xia, N., Zhou, B., Huang, N., Jiang, M., Zhang, J., Liu, L., 2016. Biosens. Bioelectron. 85, 625–632.
Yeow, N., Tabor, R.F., Garnier, G., 2017. Sci. Rep. 7, 41956.